Electronic Supplementary Material (ESI) for Food & Function.

The signatures of liver metabolomics and gut microbiota in high-fat diet fed mice supplemented with rhododendrol

Xiaoping Li[1], Yu Wang[1], Chengwei Yu[2], Yexuan Yao[1], Xi Chen[3], Ze-Yuan Deng[1], Zhao Yao[4,*], Ting Luo[1,*]

[1]State Key Laboratory of Food Science and Technology, Nanchang University, Nanchang, Jiangxi, 330047, China
[2]School of Health, Jiangxi Normal University, Nanchang, Jiangxi, 330022, China
[3]School of Food Science and Engineering, Wuhan Polytechnic University, Wuhan, Hubei, 430023, China
[4]Medical School of Jinggangshan University, Ji'an, Jiangxi, 343000, China

*Corresponding author:
Ting Luo
Address: State Key Laboratory of Food Science and Technology, Nanchang University, Nanchang, Jiangxi, 330047, China
Email: ting.luo@ncu.edu.cn

Zhao Yao
Address: Medical School of Jinggangshan University, Ji'an, Jiangxi, 343000, China
Email: yaozhao666@126.com

Abstract

As aromatic compounds found within red fruits and berries, Raspberry ketones (RK) has the potential for nonalcoholic fatty liver disease (NAFLD) amelioration. However, the mechanism of RK on NAFLD is obscure, and their bioactive metabolite is unknown. As the major metabolites of RK and mainly distributed in the liver, rhododendrol (RHO) is used in our current study to test whether RHO accounts for the beneficial effect of RK on NAFLD and the underlying mechanism. In a 16-week trial, RHO significantly decreased final body weight, improved serum lipid profile and ameliorated liver inflammation. Moreover, RHO changed the gut microbiota composition, including lean phenotype-related genera, such as *Bacteroides, Bilophila, Oscillibacter, Lachnospiraceae_bacterium_28_4* and *Bacteroides sartorii*. Liver metabolomics analysis indicated that RHO enhanced the abundance of metabolites related to alanine, aspartate, and glutamate metabolism, as well as arginine and proline metabolism. Spearman correlation analysis revealed that these metabolites were positively correlated with the gut genera enriched by RHO. Here, our findings suggested that the metabolic effects of RK might partially attributed to its metabolite-RHO, and mice supplemented with RHO dramatically alters hepatic metabolism concurrent with shifts in specific gut bacteria.

Keywords

Rhododendrol, NAFLD, Liver Metabolomics, Gut Microbiota, Amino Acid Metabolism

Introduction

Nonalcoholic fatty liver disease (NAFLD) is associated with liver metabolic reprogramming, resulting in excessive accumulation of liver lipids and imbalance of lipid metabolism [1]. Despite the high prevalence of NAFLD, no effective treatment has been proposed for it up to now. Novel food and food compounds interventions for the prevention and treatment of NAFLD have attracted attention as a potential approach to address this health problem.

Growing evidence shows that Raspberry ketone (4-(4-hydroxyphenyl) butan-2-one, RK) has the potential to protect rodents from high-fat diet induced liver damage and NAFLD [2-4]. But these effects were due to raspberry ketone itself or partially attributed by its secondary metabolites in the body has not been well investigated. Based on our preliminary data and reported study [5], we found rhododendrol (4-(4-hydroxyphenyl)-2-butanol, RHO) (Figure 1) is the main metabolites of raspberry ketone, and it is mainly distributed in the liver, after RK oral administration. Therefore, in our study, we aimed to elucidate whether RHO possess anti-NAFLD effect.

Recent studied found that the gut microbiota plays a crucial role in the development of NAFLD [6]. Dysbiosis of gut microbiota increases intestinal permeability and may increase liver exposure to harmful substances, thereby increasing liver inflammation and oxidative stress, which are the main characteristics of NAFLD. Meanwhile, the gut microbiota has important influences on host health based on its metabolites and pharmacological activities, notably bile acids, short-chain fatty acids and amino acids, which have been extensively investigated [7, 8]. Therefore, the impact of RHO on gut microbiota was investigated in the current study as well.

In this study, the effect of RHO on high-fat diet induced NAFLD were investigated. Liver metabolomics were determined to clarify RHO supplementation on the liver metabolism. Besides, the alteration on gut microbiota was evaluated after RHO administration. Furthermore, relation between shifts in the gut microbiome and hepatic metabolites were discussed to enable the identification of candidate microbes and metabolites that could help explain RHO–associated alteration in liver function in mice model of NAFLD.

Materials and Methods

Standards and Reagents

Raspberry ketone (4-(4-hydroxyphenyl)-2-butanone; 99%); rhododendrol (4-(4-hydroxyphenyl)-2-butanol; 99%), β-glucuronidase and ascorbic acid were purchased from Sigma Aldrich (St. Louis, MO, USA). LC-MS grade acids and solvents including glacial acetic acid (AA), formic acid, acetonitrile (ACN), methanol (MeOH), and ethyl acetate were from Fisher Scientific (Pittsburgh, PA, USA).

Animals

All the animal experiments in the present study were approved by the Ethical Committee of Experimental Animal Care of Nanchang University (Permit Number: 0064257). C57BL/6J male mice were purchased from Skbex Biotechnology (An'yang,

China). Male C57BL/6J mice (6 weeks old) were housed in a room maintained at 22 ± 2℃ with 40-50% relative humidity and a 12 h light/dark cycle. The mice were given free access to water and a commercial normal diet for 1-week acclimation period.

Pharmacokinetic Studies

Animal Design and Treatment

Sixty-four mice fed a low-fat diet (LFD, 10% energy from fat) were randomly divided into eight groups (8 mice in each group) for a single oral RK dose (200 mg/kg), this dose was selected based upon the previous study [5]. Following dosing, blood, liver, brown adipose tissue (BAT), white adipose tissue (WAT) and brain were collected at 5, 30 min, 1, 2, 6, and 12 h post-gavage. Vehicle dosed animals (t=0 min) were sacrificed without RK dosing to obtain the baseline. To collect samples, mice were first anesthetized with isoflurane. Blood was then collected via cardiac puncture into heparinized tubes and centrifuged at 3000 × g for 10 min at 4 °C to isolate plasma. Following cardiac puncture, animals were exsanguinated, perfused with 0.9% saline and decapitated, and tissues were collected. Tissues were immediately homogenized with 0.2% formic acid at 1:2 w/v. Plasma were acidified with 2% formic acid to a final concentration of 0.2% v/v immediately upon collection. All biological specimens were stored at −80 °C until analysis.

Extraction of RK and RHO in Biological Samples

The methods of extraction of RK and RHO were carried out according to previous study [5]. Briefly, all specimens were thawed on ice, 4-hydroxybenzoic-2,3,5,6-d4 (internal standards, 2 μg/mL), was first diluted in 0.4 m NaH_2PO_4 buffer (pH 5.4) and then added to an aliquot of plasma (100 μL), and tissue homogenate (500 μL), to a final concentration of 200 ng/mL. The mixture was mixed with 300 μL (for plasma) or 500 μL (for tissue) of NaH_2PO_4 buffer and then digested with 100 μL (plasma) or 200 μL (tissue) of the solution of β-glucuronidase (2000 U) in contamination with sulfatase diluted in NaH_2PO_4 buffer at 37 °C for 45 min after purging with nitrogen. Enzymatic reaction was stopped by adding ethyl acetate (500 μL) and mixed by vertexing vigorously for 1 min, followed by centrifugation at 8000 × g for 5 min. The upper organic phase was transferred to a disposable glass tube, followed by adding 20 μL of 2% ascorbic acid in methanol. After two more rounds of extractions with ethyl acetate (500 μL each), the pooled supernatant was dried under a gentle stream of nitrogen at room temperature. The residue was reconstituted in 200 μL of 60% methanol containing 0.1% formic acid and centrifuged at 16500 × g for 15 min before analyzed by UPLC-QqQ/MS.

Instrumentation and Analytical Methods

The analyses of RK and RHO were carried out on an Agilent 1290 Infinity II UPLC system interfaced with an Agilent 6430 triple quadrupole mass spectrometer with an electrospray ionization (ESI) source (Agilent Technology, CA, USA). Chromatographic separation was achieved using a Waters Acquity UPLC BEH C18 column (4.6×250 mm, 5 μm) (Milford, MA, USA). The binary mobile phase system

consisted of phase A (0.1% AA in water) and phase B (0.1% AA in ACN). The flow rate was set at 0.40 mL/min. The gradient elution program for each run started at 5% (B%), followed by 60% at 12 min, 70% at 20 min. Mass spectral data acquisition was achieved using positive polarities. The ESI parameters were set as follows: dry gas at 300 °C with a flow rate of 12.0 L/min, nebulizer at 30 psi, nozzle voltage at +1.5 kV/−1.0 kV and capillary voltage at +3.0 kV/-3.0 kV. Identification and confirmation of target compounds were determined by comparing their MRM precursor-product ion pair transition(s) and the retention time with those of authentic standards. Quantitation was achieved with calibration curves established using the peak area ratio of analyte-to-IS of the quantifier ions.

16-Weeks Diet Intervention Trial

Animals and Design

Thirty male mice were randomly divided into three groups (10 mice in each group): (1) low fat diet (LFD, 10% energy from fat); (2) HFD group (46% energy from fat); (3) HFD with 0.2% (wt/wt) RHO for 16 weeks. The composition of each diet was shown in Supplementary material table 1. All experimental diets were stored at 4℃ and changed every 3 days. The mice body weight and food intake were monitored every week. At the end of the diet intervention, all mice were anesthetized, and blood was collected and immediately centrifuged in anticoagulant-coated tubes for later biochemical analysis. The liver, epididymal white adipose tissue (eWAT), and inguinal white adipose tissue (iWAT) were immediately collected, weighed, and stored at -80℃ prior to analysis.

Serum Biochemical Analysis

Plasma samples were obtained by centrifugation at 2000 g for 10 min. Triglycerides (TG), total cholesterol (TC), low-density lipoprotein cholesterol (LDL-C) and high-density lipoprotein cholesterol (HDL-C), aspartate transaminase (AST), and alanine aminotransferase (ALT) were measured using commercial kits (Jiancheng, Co., Nanjing, China).

Morphological of Liver

Mice liver was dissected and fixed in 10% formalin for at least 24 h. After dehydrated with ethanol and embedded in paraffin, tissues of 5 μm thickness were cut, deparaffinized, rehydrated, stained with hematoxylin and eosin (H&E) or Oil Red O, subjected to microscopic observation. The liver sections were imaged at 200× magnification and quantified by Image J software.

RNA Extraction and RT-PCR Analysis

Total RNA from liver was isolated using the Trizol reagent (Invitrogen, Carlsbad, CA). The cDNA was generated from 1μg of RNA using Takara kit (Takara, Japan). The amplification reaction mixture (10 μL) contained 5 μL of SYBR Green, 0.5 μL of reverse and forward primer, 2 μL of cDNA and 2 μL of DEPC water. The relative expression level of target genes was normalized to the housekeeping gene β-actin, and

primer sequences are listed in Supplementary materials table 2.

Untargeted Metabolomics in Liver

Metabolite Extraction

A two-step process according to previous study was used in the present study, which is based on extraction into 'aqueous' and 'organic' phases for polar and nonpolar metabolites [9]. Briefly, the collected liver samples (50 mg) were thawed on ice, and homogenized with 1.5 mL prechilled methanol/water (-80℃, 1:1 V:V) in bead-beater tubes. Then, the tubes were centrifuged at 14000 g for 10 min at 4℃, and the supernatant was transferred to a fresh tube following with drying in vacuum concentrator. The retained sediment in the tube was used for extraction of 'aqueous' phase. 1.6 mL of mix solution of dichloromethane/methanol (-80℃, 3:1 V:V) was added to the remaining sediment, following with homogenization the tissue and centrifuge the mixture at 14000 g for 10 min and collected the supernatant into a new glass vial at 4℃. All the dried 'aqueous' and 'organic' samples were dissolved in 120 μL MeOH:H_2O (1:1) solution for LC-MS analysis. Pooled quality control (QC) samples were prepared by combing 15 μL of each extraction samples.

LC-MS Analysis

All samples from each group (n = 5) were analyzed using a UPLC-Q-Exactive-MS equipped with an electrospray ion source (HESI) and Xcalibur 4.1 software (Thermo-Fisher, USA) with both positive and negative ion modes. An Acquity UPLC BEH C18 (2.1 mm × 50 mm, 2.2 μm) was used for reversed-phase separation. The mobile phase consisted of solvent A (water, 0.1% formic acid) and solvent B (ACN, 0.1% formic acid). The gradient elution conditions were as follows with a flow rate of 0.3 ml/min: 10-25% solvent B for 0-4 min; 25-55% solvent B for 4-7 min; 55-100% solvent B for 7-28 min; 100 solvent B for 28-29 min; and 100-10% solvent B for 29-30 min. Column temperature was maintained at 30℃.

The Q-Exactive-MS system was used to detect metabolites eluted from the column. In this mode, the acquisition software continuously evaluates the full scan MS spectrum. The ESI source conditions were set as follows: sheath gas flow rate of 50 Arb, Aux gas flow rate of 10 Arb, capillary temperature of 320℃, full MS resolution of 70000, MS/MS resolution of 17500, collision energy of 15/30/45 in NCE mode, and spray voltage of 3.5 kV (positive) or -3.2 kV (negative).

Bioinformatic Analysis

Principal component analysis (PCA) and Orthogonal partial least squares discriminant analysis (OPLS-DA) were employed in the present study to analyze the difference of serum metabolites in different groups, and the over fitting of the model is verified by cross-validation (permutation test) using SIMCA-P (16.0.2, Sartorius Stedim Data Analytics AB, Umea, Sweden). Then, univariate statistical analysis was used to screen metabolic markers with significant differences. Briefly, based on OPLS-DA, the variable importance in the projection (VIP)>1, and a p value <0.05 were defined as differences. Furthermore, the significantly changed metabolite pathways were analyzed

using the KEGG database (Kyoto Encyclopedia of Genes and Genomes).

Gut Microbiota Analysis

Fecal samples collected from cecum were used to isolate total bacterial DNA according to the manufacturer's protocol. The extracted DNA samples were stored at -80℃ after measured for concentration using the NanoDrop ND-1000 spectrophotometer (Nano-Drop Technologies, Wilmington, DE). Specific primer set (341F, 805R) were used to amplify the V3-V4 region of the 16s rRNA gene in a Hiseq sequencing platform (Illumina). The PCR products were purified and quantified with a Mini Elute PCR purification kit (AXYGEN) and ABI GeneAmpI 9700 system, respectively. Sequencing was accomplished on the Illumina HiSeq platform according to the standard protocol. Data were read by FLASH V.1.2.7 software to obtain splicing sequence, namely primitive Tags data. Then, Trimmomatic V0.33 software was utilized to collect high-quality Tags data from the Mosaic. The final valid data were acquired by UCHIME V4.2 software after verifying and getting rid of chimeric sequences.

Statistics

Data are presented as means ± SEM. ANOVA was used to compare sets of data. Tukey's test was used for the post hoc testing. All statistical analyses were carried out using GraphPad Prism. $P<0.05$ was considered as significant. The correlation between gut microbiota and liver metabolites was determined by Spearman correlation analysis.

Results

Plasma Pharmacokinetics and Tissue Distribution of RK and RHO in Mice

Representative LC-MS chromatograms of RK and RHO detected in plasma and tissues of mice was shown in Figure 1A, and the concentration of RK and RHO at specific time post-administration were shown in Figure 1B. In a 12-h trial period, the peak times of both RK and RHO in plasma were at 5 min, suggesting the quick absorption and conversion while the peak value of RHO was nearly half that of RK (100.9±19.5 *vs.* 241.2±42.9 nmol/mL). As shown in Figure 1C and 1D, the distribution of RK and RHO in different tissues were also detected. In accordance with plasma, the peaking times of RK and RHO also arrived at 5 min post administration in tissues, and the highest peaking concentration were both observed in liver, followed by BAT, WAT and brain.

Effects of Rhododendrol on Body Weight Gain and Body Fat in HFD-Fed Mice

Male C57BL/6J mice aged 6 weeks were fed either normal diet (LFD group) or high fat diet (HFD group) or high-fat plus 0.2% rhododendrol (HFD+RHO group) for 16 weeks. The data showed that HFD group mice exhibited significantly increased body weight compared with the LFD group and HFD+RHO group, and no significant differences of final weight were observed between LFD group and HFD+RHO group. However, RHO intervention did not significantly affect changes in food intake or total energy intake in HFD-fed mice. Furthermore, HFD increased the liver, epididymal fat and inguinal fat weight, and RHO intervention inhibited high fat diet induced organ

index gain (Figure 2).

Effects of Rhododendrol on Blood Lipid Profiles and Liver Function

Total TG, TC, HDL-C, LDL-C, ALT, AST in the three groups were measured at the end of 16-week trial. Mice in the HFD group showed significantly higher TG, TC, LDL-C, AST and ALT levels in serum when compared with LFD group, and the treatment of rhododendrol reversed these effects, although no difference of HDL-C was observed between HFD group and HFD+RHO group (Table 1).

H&E and oil red O staining of liver tissue showed that more lipid droplets were found in HFD mice, compared with LFD group. RHO treatment reduced the proportion of lipid area. These results suggested that the intake of RHO effectively inhibited the accumulation of lipid in liver and ameliorated liver damage induce by HFD (Figure A, C).

Moreover, the mRNA levels of proinflammatory cytokines including tumor necrosis factor-a (TNF-a), interleukin-1β (IL-1β), monocyte chemoattractant protein 1 (MCP1), and IL-6 were significantly decreased by RHO treatment when compared with HFD group (Figure 3D).

Effects of Rhododendrol Supplementation on Liver Metabolomes

To identify how HFD and RHO affect the liver function, untargeted metabolomics with both positive and negative models were employed to investigate the influence of rhododendrol on liver metabolites. The PCA and OPLS-DA results showed distinguishable liver metabolites between high fat-fed mice and RHO-fed mice (Figures 4A, 4B). The permutation test showed that all OPLS-DA models were reliable without overfitting (Figure 4C). The volcano plot (Figure 4D) showed significant changes of liver metabolites after treatment with HES. Based on volcano plot, we found 249 metabolites were significantly increased and 38 metabolites were decreased after RHO intervention.

Furthermore, we combined OPLS-DA and t-test to screen key small molecular metabolites that may be regulated by RHO. The top 50 metabolites (VIP＞1 and p＜ 0.05) were shown in Figure 5. In HFD group, few compounds, including adenine and guanine were significantly enriched, which were involved in nucleotide metabolism. On the other hand, most of the metabolites were enriched in RHO group, such as L-(+)-aspartic acid which was associated with aspartate metabolism, D-proline and ornithine were involved in arginine and proline metabolism.

Effects of Rhododendrol on Alteration of the Metabolic Pathway in HFD-Fed Mice

Based on the PCA and OPLS-DA results, the relative abundance of metabolites in liver between HFD and HFD + RHO mice were shown to be significantly different. Thus, relevant metabolic pathways were further analyzed using significant difference metabolites between these two groups (VIP＞1 and p＜0.05) (Figure 6). The data indicated that the RHO mainly affect the aminoacyl-tRNA biosynthesis, alanine, aspartate and glutamate metabolism, arginine and proline metabolism, and

phenylalanine, tyrosine and tryptophan biosynthesis, etc.

Effects of Rhododendrol on Gut Bacterial Community in Mice

The effect of RHO on gut microbiota composition was analyzed through 16S rRNA sequencing (v3-v4 region) of mice feces. PCoA analysis demonstrated distinct clustering of gut microbiota composition among the LFD, HFD and HFD+RHO groups (Figure 7A), indicating that different diets and RHO supplementation promoted the variance of the gut microbial populations. This changes among different groups were also confirmed by the NMDS plot analysis (Figure 7B). At the phylum level, a total of 10 phyla were defined in our study, and *Bacteroidetes* and *Firmicutes* were the primary phyla among all the groups. HFD significantly increased the relative abundance of *Firmicutes* and decreased the *Bacteroidetes* (Figure 7C), while the intervention of RHO robustly increased the abundance of *Bacteroidetes* and decreased the ratio of *Firmicutes* to *Bacteroidetes* (Figure 7D).

Next, linear discriminant analysis effect size (LEfSe) analysis was performed to identify the characteristic bacteria of each group. Our results indicated that a total of 42 operational taxonomic units (OUTs) were notably different among these three groups and there are 11, 9 and 22 significant differences in the HFD, LFD and HFD+RHO groups, respectively. Particularly, HFD significantly increased the relative abundance of *p_Firmicutes*, *c_Bacilli*, and *o_Erysipelotrichales*, etc. Under HFD condition, the supplementation of RHO increased the abundance of o*_Bacteroidales, p_Campylobacterota* and *f_Helicobacteraceae,* etc. (Figure 8A). The marker taxa between HFD and RHO groups were also confirmed by T-test analysis at genus level (Figure 8B) and species level (Figure 8C).

Rhododendrol Changes the Overall Function of Gut Microbiota

The gut functional changes caused by RHO treatment were predicted by Phylogenetic Investigation of Communities by Reconstruction of Unobserved States (PICRUSt) and was exhibited in Figure 8D. Our results indicated that, based on the Kyoto Encyclopedia of Genes and Genomes (KEGG) analysis, RHO supplementation remarkably altered the microbial function between HFD and HFD+RHO groups, in which pyruvate metabolism, arginine and profline metabolism, alanine, aspartate and glutamate metabolism were enriched in RHO group.

Moreover, we investigated the relation between key changed microbiota communities and phenotype parameters in mice (Figure 9), and we found that genus *Faecalibaculum*, *Lactobacillus*, *Blautia* and *Roseburia* were predicted to positively correlated with most of the phenotype parameters, but genus *Parabacteroides*, *Bacteroides* and *Biophila* showed the reverse trend.

Collectively, these results demonstrated that RHO has a role in shaping the gut microbial composition and altering its overall function.

Correlation of Key Microbiota Communities and Differential Liver Metabolites

To investigate the relationship between gut microbiota and liver metabolites, Spearman correlation analysis was conducted between the seven genera enriched by RHO (based

on T-test analysis results) and the liver metabolites changed by RHO treatment (p<0.05 and VIP＞1, top 50) (Figure 10). All the eight bacteria tend to be positively correlated with the metabolites up-regulated by RHO administration, but the bacteria *g_Alistipes* and *s_Bacteroides_acidifaciens* were only significantly correlated with a few liver metabolites, suggestion their weak correlations. Meanwhile, adenine and guanine, which were down-regulated in RHO group, were negatively correlated with these bacteria.

Discussion

In the present study, we analyzed the metabolites of RK and metabolites distribution in different tissues. Our data reveled that RHO was one of the major metabolites of RK. Following acute RK administration, the concentration of RHO in liver was the highest among all organs, suggestion its possible target tissue.

In order to test whether RHO accounts for the beneficial effect of RK on NAFLD and the underlying mechanism, the weight control and hepatic protection effects of RHO were investigated in HFD-induced NAFLD mice model. We then integrated gut microbiota and untargeted liver metabolites analysis to uncover its beneficial effects on combating obesity and hepatic protection in a high fat-induced NAFLD model.

After a 16-week trial, we found that RHO deceased the final body weight, liver and epididymal fat weight, serum lipid level, ALS, and AST levels. It also decreased lipid accumulation in liver without influencing the food intake and energy intake when compared with high-fat diet group. The supplementation of RHO in the mice diet was 0.2% (wt/wt), which was based on the equivalent dose of RK used in the previous study [10] and is equivalent to 800 mg/50kg B.W. of human, which is achievable for human dietary supplement consumption.

Through integrated analysis of gut microbiota and liver metabolome data, some specific gut bacteria species and liver metabolite were identified in our results that were considered benefit from the RHO treatment, which might contribute to improved metabolic status.

The results of gut microbiome analysis showed that *Firmicutes* was the most dominant phylum among all groups, which are responsible for energy resorption and obesity. Phyla *Firmicutes* and *Bacteroides* account for more than 90% of all the bacterial species in human gut [11, 12]. The change in the ratio of these two bacterial was highly associated with weight change, and a high ratio of *Firmicutes* to *Bacteroidetes* was found in obese individuals [12]. Numerous studied have pointed out that a relative increase ratio of *Firmicutes* to *Bacteroides* was highly related with obesity and phytochemicals were effective to rebalance these two bacterial. For example, mice fed an HFD with 200 mg/kg/day pomegranate fruit pulp polyphenols (PFP) for 14 weeks significantly reduced the body weight, accompanied with increasing of the abundance of phylum *Bacteriodetes* and decreased the relative abundance of *Firmicutes* [13]. In the present study, remarkably differences of microbiota composition were observed in different groups. The ratio of the *Firmicutes* to *Bacteroidetes* was significantly increased by HFD feeding, and RHO supplementation reversed this effect, which indicated another possible mechanism of how RHO combats obesity.

Besides *Bacteroides*, we also identified seven other specific genera after RHO treatment. In which, *Bilophila* has been reported to be a key taxa in the process of α-linolenic acid-improved multi-tissue homeostasis in HFD mice, because it showed negatively correlation with metabolic disorders and positively correlation with most beneficial indicators [14]. *Oscillibacter* [15], *Lachnospiraceae_bacterium_28_4* [16], *bacteroides sartorii* [17] were also reported to be lean-related genera, and alistipes was noted as an obesity-related taxa [18]. Overall, these data demonstrated that RHO administration selectively enriches some gut bacteria, which might contribute to its anti-obesity and liver protection effects.

High fat diet intervention could dramatically change the liver metabolic profile. Yang[19] reported that rats fed with HFD (40% fat, 42% carbohydrate and 18% protein) for 4 weeks significantly increased the levels of TG, diacylglycerol (DG), phosphatidyl inositols (PI), phosphatidyl glycerol (PG) and phosphatidyl serines (PS) of liver when compared to normal chow diet (12% fat, 60% carbohydrate and 28% protein) group. Meanwhile, levels of some kinds of bile acids (cholic acid, deoxycholic acid, and taurocholic acid) were also elevated after HFD supplementation. In addition to the liver, a high-fat diet can also affect the metabolomic changes in blood and urine. Maria and colleagues demonstrated that following a diet containing 41% fat, 49% carbohydrate and 10% protein, the urinary excretions of citrate, glycerophosphocholine (GPC), sucrose, N-methyl-4-pyridone-3-carboxamide(4-PY), and metabolites related to inflammation and oxidative stress (N-acetylglycoproteins [NAG], 2'-deoxycitidine) were increased when compared to a standard diet, and higher serum levels of branched chain amino acid (BCAA) and branched chain keto acids (BCKA) (3-methyl-2-oxovalerate [2-MOV]) were observed in high-fat treated mice.[20]

Regarding the potential target organ of RHO might be liver, we discovered the influences of RHO on liver metabolism through metabolome analysis. Based on the KEGG pathway enrichment analysis, the RHO diet mainly affected amino acid metabolism. The top 50 differential metabolites between HFD group and HFD plus RHO mice involved in these pathways were also identified. For example, L-(+)aspartic acid was involved in the pathway of alanine, aspartate and glutamate metabolism pathway, D-proline and ornithine were participated in arginine and proline metabolism, and these metabolites were all enriched after RHO supplementation.

Intriguingly, we compared the KEGG pathways affected by gut microbiota and liver metabolites, and we found the coincidence of the pathways both involved in the two eco-system, such as alanine, aspartate and glutamate metabolism pathway and arginine and proline metabolism pathway, suggestion the correlation between gut microbiota shift and liver function. The correlation between amino acid metabolism in the gut and metabolic disease has been demonstrated in previous study [21], the author found the supplementation of citrus polymethoxyflavones attenuate metabolic syndrome by regulating gut microbiome and reducing the biosynthesis of branched-chain amino acid in host faces and serum. Aspartate is known as major intermediate in the citrate cycle, which was reported to attenuate metabolic disorders after administration in *vitro* or in mice, and its content in liver was up-regulated by oral gavage of bacterium *Akkermansia muciniphila* in a high-fat and high-cholesterol (HFC)

diet induced obese mice model [22]. L-arginine (7.2-fold increased, data not show) is a functional amino acid and a precursor of nitric oxide, which plays a crucial role in animal maintenance, reproduction, growth, anti-aging and immunity. Growing clinical evidence suggests that dietary L-arginine supplementation reduces obesity, decrease blood pressure, and modulates endothelial dysfunction, thereby alleviating type 2 diabetes [23]. These results suggested the anti-obesity and hepatic protection effects of RHO might through gut-liver axis.

In summary, RHO intervention improved HFD-induced NAFLD by selectively enriched a group of gut bacteria which have been proved to ameliorate NAFLD and related metabolic syndrome, such as *Bacteroides, Oscillibacter, Lachnospiraceae_bacterium_28_4* and *Bacteroides sartorii,* and the beneficial activity of RHO was correlated with improved gut-liver interaction through regulating the alanine, aspartate and glutamate metabolism and arginine and proline metabolism pathways. Also, this study demonstrated that it is of value to study the metabolites of phytochemicals, since the metabolites might serve as the bioactive forms as well.

Ethical statement

The authors state that all experiments were performed in compliance with the relevant laws and institutional guidelines. The informed consent is exempted with the consent of the ethics committee of Experimental Animal Care of Nanchang University (Permit Number: 0064257).

Acknowledgments

This work was financially supported by the National Natural Science Foundation of China (Grant No. 82160168), “Shuangqian Project" of Scientific and Technological Innovation of High-end Talents-Natural Science, Jiangxi Province (Grant No. jxsq2020101063), Natural Science Foundation of Jiangxi Province (Grant No. 20212BAB216075), and Central Government Guide Local Special Fund Project for Scientific and Technological Development of Jiangxi Province (Grant No. 20221ZDD02001).

References

1. N. M. de Alwis and C. P. Day, Non-alcoholic fatty liver disease: the mist gradually clears, *Journal of hepatology*, 2008, **48 Suppl 1**, S104-112.
2. T. Luo, O. Miranda-Garcia, G. Sasaki and N. F. Shay, Consumption of a single serving of red raspberries per day reduces metabolic syndrome parameters in high-fat fed mice, *Food & function*, 2017, **8**, 4081-4088.
3. L. Wang, X. Meng and F. Zhang, Raspberry ketone protects rats fed high-fat diets against nonalcoholic steatohepatitis, *J Med Food*, 2012, **15**, 495-503.
4. X. Li, T. Wei, M. Wu, F. Chen, P. Zhang, Z. Y. Deng and T. Luo, Potential metabolic activities of raspberry ketone, *Journal of food biochemistry*, 2022, **46**, e14018.
5. D. Zhao, B. Yuan, D. Kshatriya, A. Polyak, J. E. Simon, N. T. Bello and Q. Wu, Influence of Diet-Induced Obesity on the Bioavailability and Metabolism of Raspberry Ketone (4-(4-

Hydroxyphenyl)-2-Butanone) in Mice, *Molecular nutrition & food research*, 2020, **64**, e1900907.

6. C. Leung, L. Rivera, J. B. Furness and P. W. Angus, The role of the gut microbiota in NAFLD, *Nature reviews. Gastroenterology & hepatology*, 2016, **13**, 412-425.
7. Y. Fan and O. Pedersen, Gut microbiota in human metabolic health and disease, *Nature reviews. Microbiology*, 2021, **19**, 55-71.
8. A. Agus, K. Clément and H. Sokol, Gut microbiota-derived metabolites as central regulators in metabolic disorders, *Gut*, 2021, **70**, 1174-1182.
9. E. J. Want, P. Masson, F. Michopoulos, I. D. Wilson, G. Theodoridis, R. S. Plumb, J. Shockcor, N. Loftus, E. Holmes and J. K. Nicholson, Global metabolic profiling of animal and human tissues via UPLC-MS, *Nature protocols*, 2013, **8**, 17-32.
10. S. Y. Leu, Y. C. Tsai, W. C. Chen, C. H. Hsu, Y. M. Lee and P. Y. Cheng, Raspberry ketone induces brown-like adipocyte formation through suppression of autophagy in adipocytes and adipose tissue, *The Journal of nutritional biochemistry*, 2018, **56**, 116-125.
11. P. B. Eckburg, E. M. Bik, C. N. Bernstein, E. Purdom, L. Dethlefsen, M. Sargent, S. R. Gill, K. E. Nelson and D. A. Relman, Diversity of the human intestinal microbial flora, *Science (New York, N.Y.)*, 2005, **308**, 1635-1638.
12. P. J. Turnbaugh, R. E. Ley, M. A. Mahowald, V. Magrini, E. R. Mardis and J. I. Gordon, An obesity-associated gut microbiome with increased capacity for energy harvest, *Nature*, 2006, **444**, 1027-1031.
13. H. Song, X. Shen, Q. Chu and X. Zheng, Pomegranate fruit pulp polyphenols reduce diet-induced obesity with modulation of gut microbiota in mice, *Journal of the science of food and agriculture*, 2021, DOI: 10.1002/jsfa.11535.
14. X. Gao, S. Chang, S. Liu, L. Peng, J. Xie, W. Dong, Y. Tian and J. Sheng, Correlations between α-Linolenic Acid-Improved Multitissue Homeostasis and Gut Microbiota in Mice Fed a High-Fat Diet, *mSystems*, 2020, **5**.
15. M. Raman, I. Ahmed, P. M. Gillevet, C. S. Probert, N. M. Ratcliffe, S. Smith, R. Greenwood, M. Sikaroodi, V. Lam, P. Crotty, J. Bailey, R. P. Myers and K. P. Rioux, Fecal microbiome and volatile organic compound metabolome in obese humans with nonalcoholic fatty liver disease, *Clinical gastroenterology and hepatology : the official clinical practice journal of the American Gastroenterological Association*, 2013, **11**, 868-875.e861-863.
16. X. Li, T. Wei, J. Li, Y. Yuan, M. Wu, F. Chen, Z. Y. Deng and T. Luo, Tyrosol ameliorates the symptoms of obesity, promotes adipose thermogenesis, and modulates the composition of gut microbiota in HFD fed mice, *Molecular nutrition & food research*, 2022, DOI: 10.1002/mnfr.202101015, e2101015.
17. M. A. G. Hernández, E. E. Canfora, J. W. E. Jocken and E. E. Blaak, The Short-Chain Fatty Acid Acetate in Body Weight Control and Insulin Sensitivity, *Nutrients*, 2019, **11**.
18. J. Zhu, Y. Kong, J. Yu, S. Shao, M. Mao, M. Zhao and S. Yue, Consumption of drinking water N-Nitrosamines mixture alters gut microbiome and increases the obesity risk in young male rats, *Environmental pollution (Barking, Essex : 1987)*, 2019, **248**, 388-396.
19. J. Yang, H. Chen, Q. Nie, X. Huang and S. Nie, Dendrobium officinale polysaccharide ameliorates the liver metabolism disorders of type II diabetic rats, *Int J Biol Macromol*, 2020, **164**, 1939-1948.
20. M. Guirro, A. Gual-Grau, A. Gibert-Ramos, J. M. Alcaide-Hidalgo, N. Canela, L. Arola and J.

Mayneris-Perxachs, Metabolomics Elucidates Dose-Dependent Molecular Beneficial Effects of Hesperidin Supplementation in Rats Fed an Obesogenic Diet, *Antioxidants (Basel, Switzerland)*, 2020, **9**.

21. S. L. Zeng, S. Z. Li, P. T. Xiao, Y. Y. Cai, C. Chu, B. Z. Chen, P. Li, J. Li and E. H. Liu, Citrus polymethoxyflavones attenuate metabolic syndrome by regulating gut microbiome and amino acid metabolism, *Science advances*, 2020, **6**, eaax6208.
22. Y. Rao, Z. Kuang, C. Li, S. Guo, Y. Xu, D. Zhao, Y. Hu, B. Song, Z. Jiang, Z. Ge, X. Liu, C. Li, S. Chen, J. Ye, Z. Huang and Y. Lu, Gut Akkermansia muciniphila ameliorates metabolic dysfunction-associated fatty liver disease by regulating the metabolism of L-aspartate via gut-liver axis, *Gut microbes*, 2021, **13**, 1-19.
23. S. Hu, M. Han, A. Rezaei, D. Li, G. Wu and X. Ma, L-Arginine Modulates Glucose and Lipid Metabolism in Obesity and Diabetes, *Current protein & peptide science*, 2017, **18**, 599-608.

Figures and Legends:

Table 1. Plasma parameters of mice fed LFD, HFD or HFD+RHO diet.

	LFD	HFD	HFD+RHO
TG (mmol/L)	0.54±0.03a	1.25±0.04b	0.92±0.11a
TC (mmol/L)	4.99±0.26a	9.41±0.18b	7.11±0.14c
HDL-C (mmol/L)	3.79±0.08a	3.57±0.09a	3.05±0.19a
LDL-C (mmol/L)	0.62±0.03a	1.47±0.04b	0.99±0.12a
AST (U/L)	85.73±3.89a	127.45±3.68b	105.58±4.85a
ALT (U/L)	28.08±0.89a	66.63±2.11b	44.21±4.54c

LFD, low fat diet; HFD, high fat diet; HFD+RHO, high fat diet plus 0.2 % (wt/wt) rhododendrol diet. Different letters represent significantly difference from each other in a row at $p < 0.05$. Values are mean ± SEM (n=10).

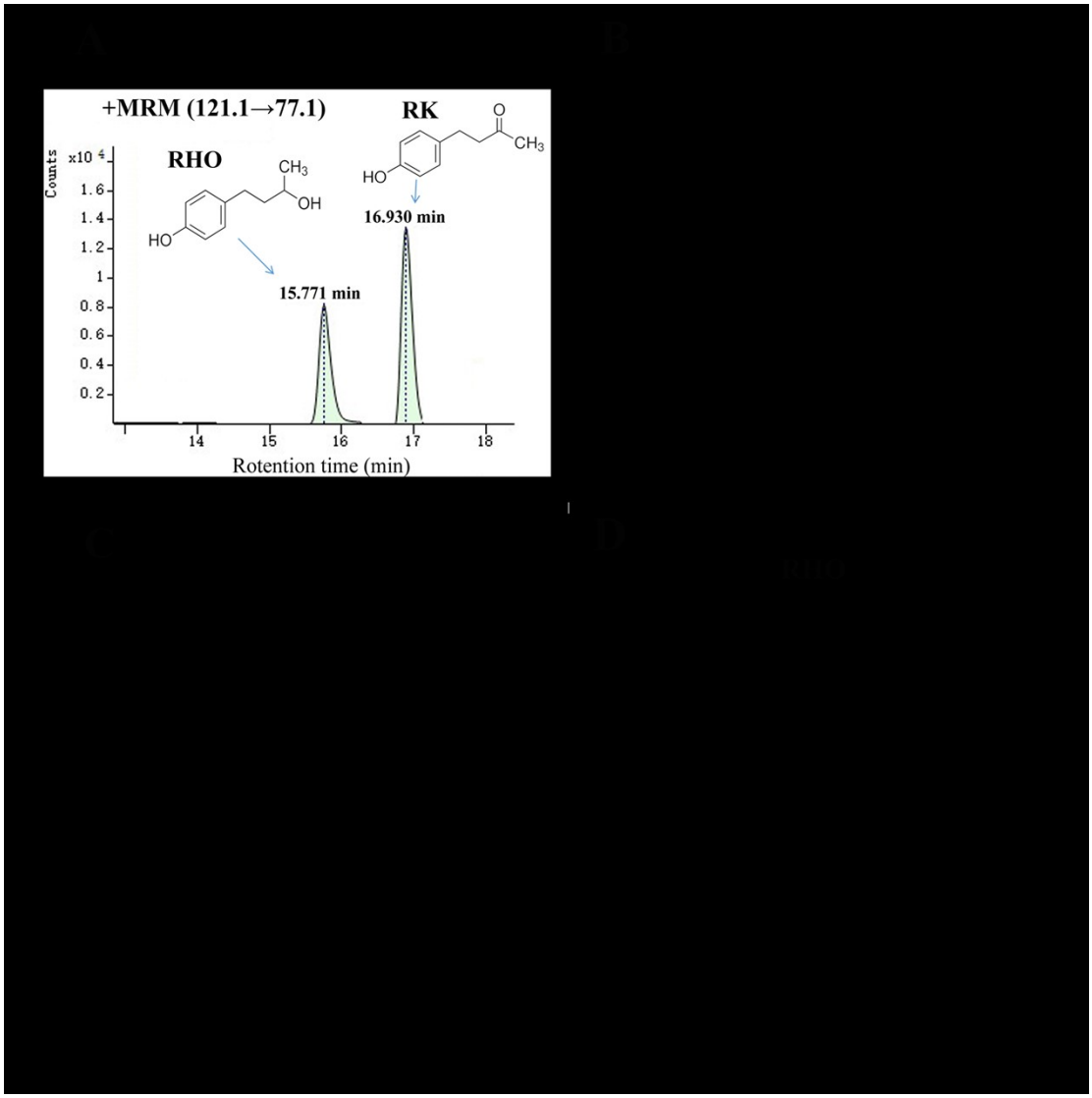

Figure 1. A. Representative MS chromatograms of RK and RHO detected in plasma of mice (samples are collected at 5 min post-gavage). Pharmacokinetic curves of raspberry ketone (RK) and raspberry alcohol (RHO) a in plasma (B), and tissues (C and D) in mice dosed with RK. Bars are mean ± SEM (n = 8).

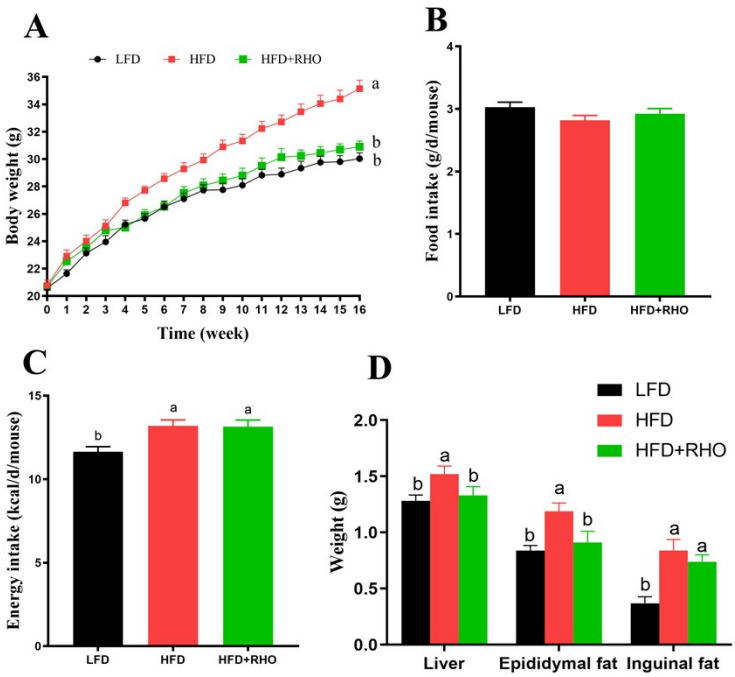

Figure 2. Body weight and tissue weight in C57BL/6J male mice fed a low-fat diet (LFD), a high fat diet (HFD), or HFD plus rhododendrol (HFD+RHO) during a 16-week feeding trial. Weekly body weight was analyzed using repeated- measures ANOVA followed by post-hoc testing within each week with one-way ANOVA. A. Body weight. B. Food intake. C. Energy intake. D. Liver, epididymal fat and inguinal fat weight. LFD, low fat diet; HFD, high fat diet; HFD+RHO, high fat diet plus 0.2 % (wt/wt) rhododendrol diet. Different superscripts (a, b) represent significantly difference from each other, $p < 0.05$. Bars are mean ± SEM (n = 10).

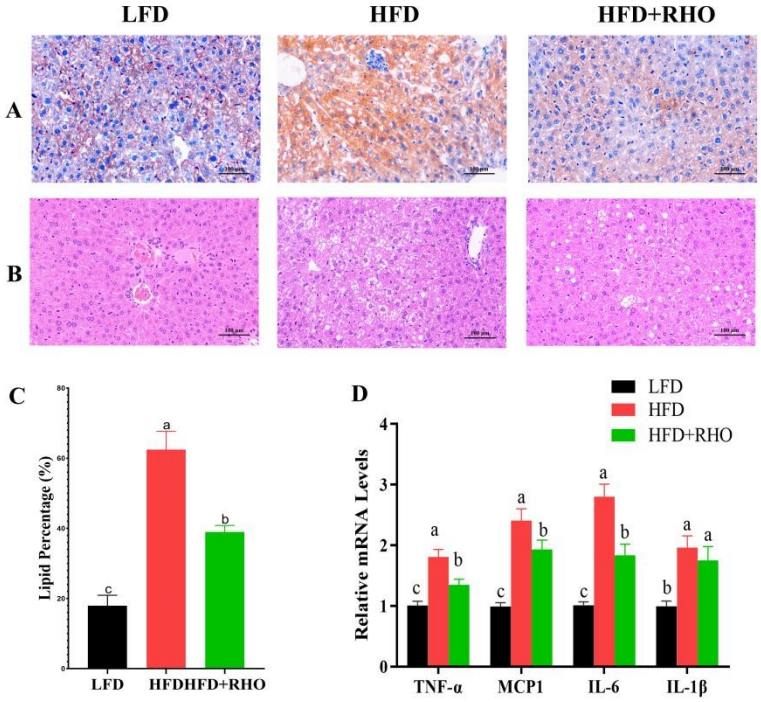

Figure 3. Effects of RHO on liver histology. A. Representative photomicrographs of oil-red stained

sections of the liver (200× magnification), red represent lipid droplets. B. Representative photomicrographs of H&E stained sections of the liver (200× magnification). C. Quantified hepatic lipid accumulation (calculated by Image J). D. mRNA expression levels of TNF-α, MCP1, IL-6 and IL-1β of the liver. LFD, low fat diet; HFD, high fat diet; HFD+RHO, high fat diet plus 0.2 % (wt/wt) rhododendrol diet. Different superscripts (a, b, c) represent significantly difference from each other, $p < 0.05$. Bars are mean ± SEM (n = 5).

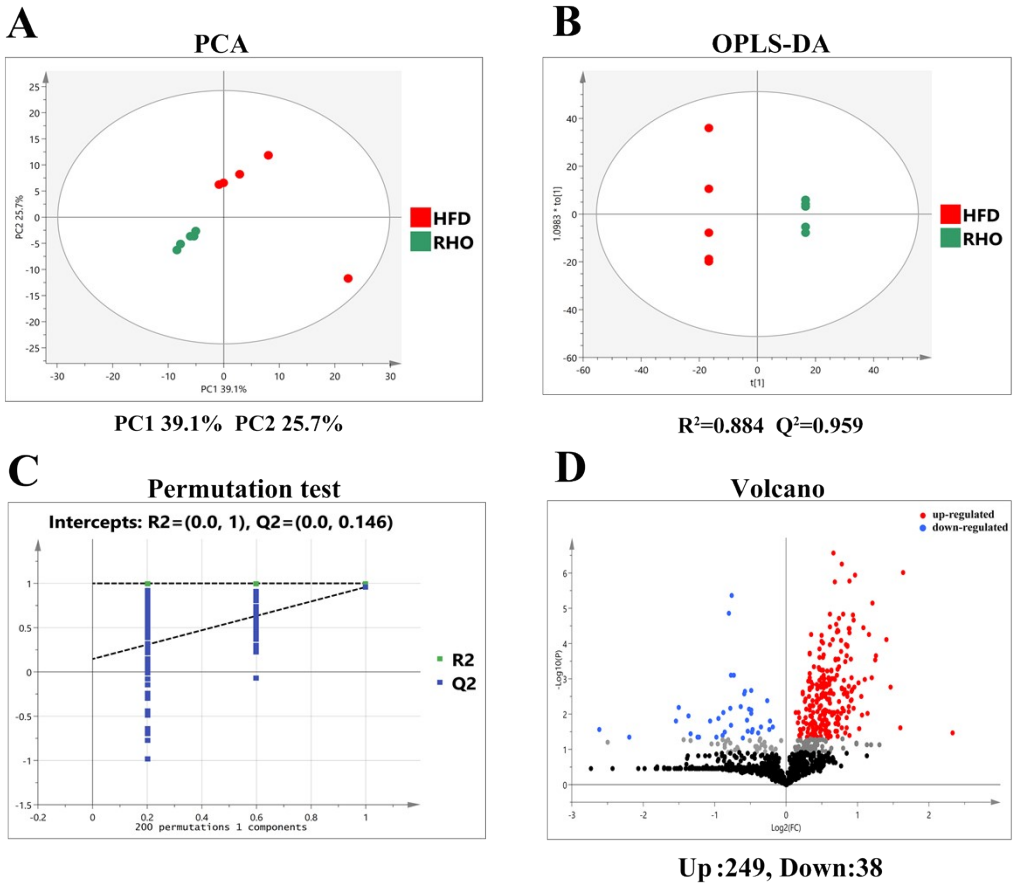

Figure 4. RHO affects the liver metabolites in mice. The principal component analysis (PCA) plot (A) and orthogonal partial least squares discrimination analysis (OPLS-DA) plot (B) based on the metabolites in the liver. C. Permutation test plot based on OPLS-DA methods. D. The volcano plot based on the changed metabolites of the HFD+RHO group compared to the HFD group. HFD, high fat diet; RHO, high fat diet plus 0.2 % (wt/wt) rhododendrol diet, n=5.

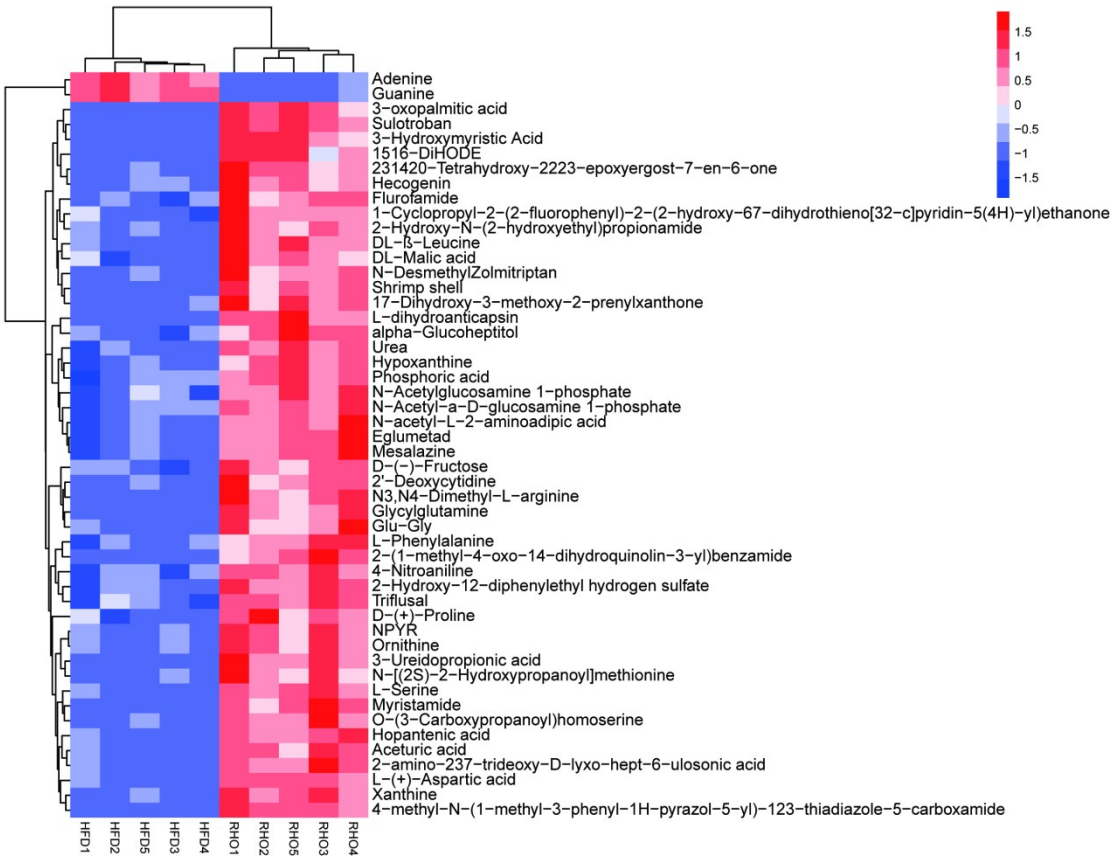

Figure 5. Heat map of the top 50 metabolites in HFD and HFD+RHO groups. HFD, high fat diet; RHO, high fat diet plus 0.2 % (wt/wt) rhododendrol diet.

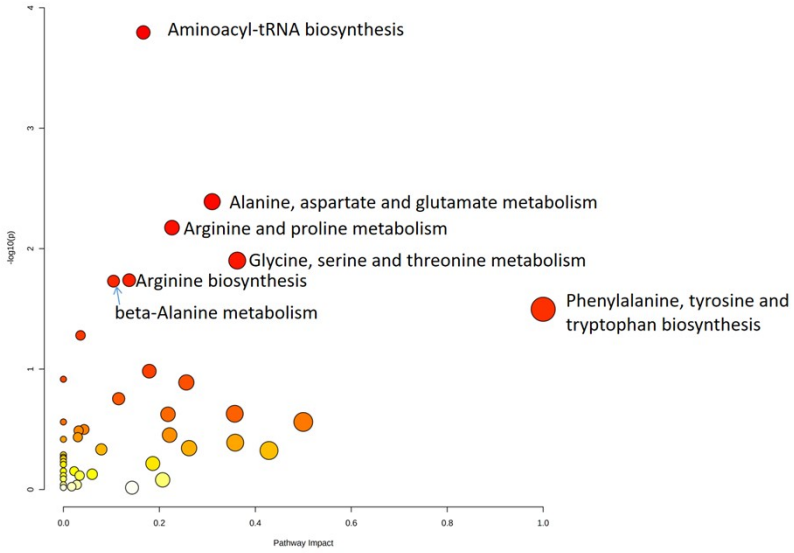

Figure 6. RHO regulates the metabolic pathways of liver in HFD-induced mice.

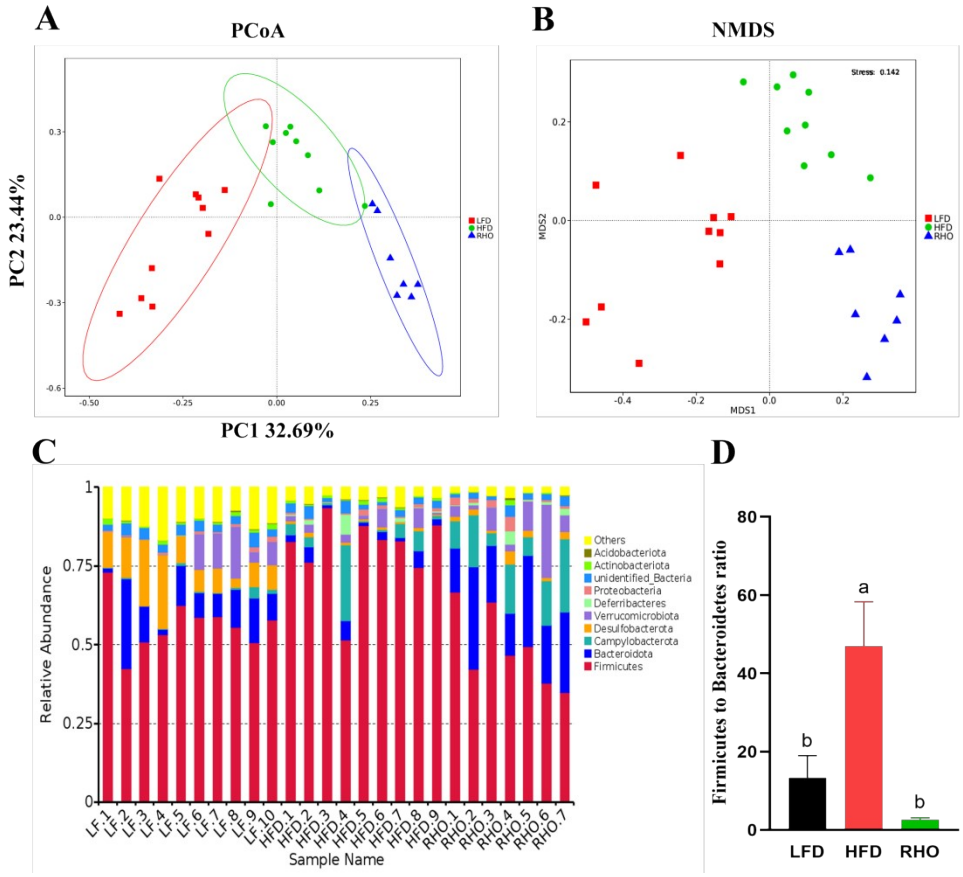

Figure 7. Effect of RHO on the gut microbial community composition. (A) Principal coordinate analysis (PCoA) of gut microbiota between all groups. (B) NMDS plots between all groups. (C) The relative abundance of the top ten abundant bacteria at the phylum level. (D) The ratio of Firmicutes to Bacteroidetes. LF represent low fat diet; HFD represent high fat diet; RHO represent high fat diet plus 0.2 % (wt/wt) rhododendrol diet. Different superscripts (a, b) represent significantly difference from each other, $p < 0.05$. Bars are mean ± SEM (n =7-10).

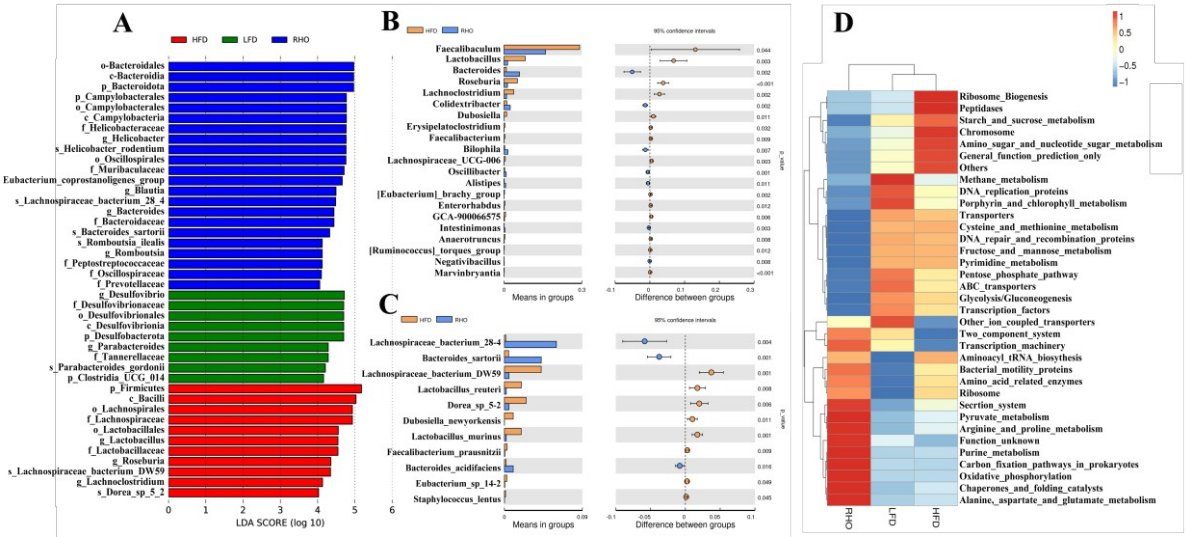

Figure 8. Linear Discriminant Analysis Effect Size (LEfSe) analysis of the characteristic genera of

gut microbiota (A). Significant differences germs between HFD and RHO groups in genus level (B) and species level (C)(T-test). PICRUSt-predicted microbial community functional changes among three groups (D). LFD represent low fat diet; HFD represent high fat diet; RHO represent high fat diet plus 0.2 % (wt/wt) rhododendrol diet, (n =7-10).

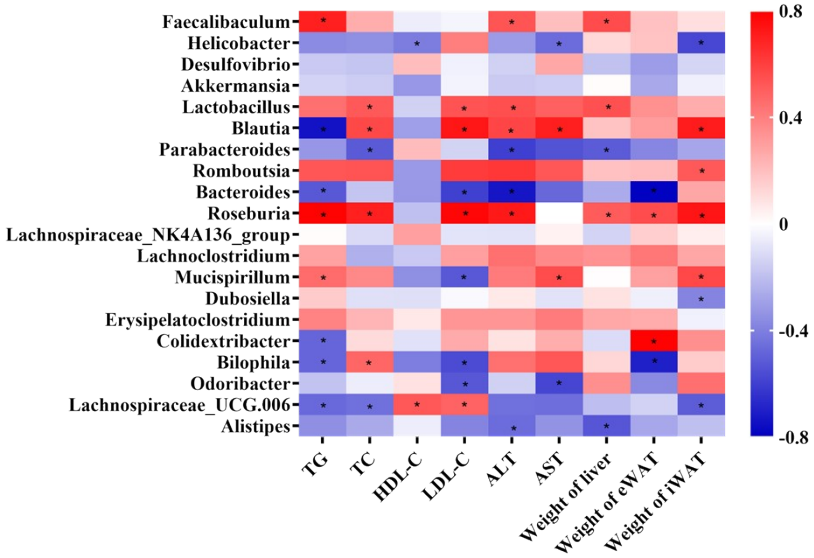

Figure 9. Heatmap of the Spearman's correlations between the bacterial genera and the metabolic parameters in mice treated with HFD alone or HFD plus RHO. *p<0.05.

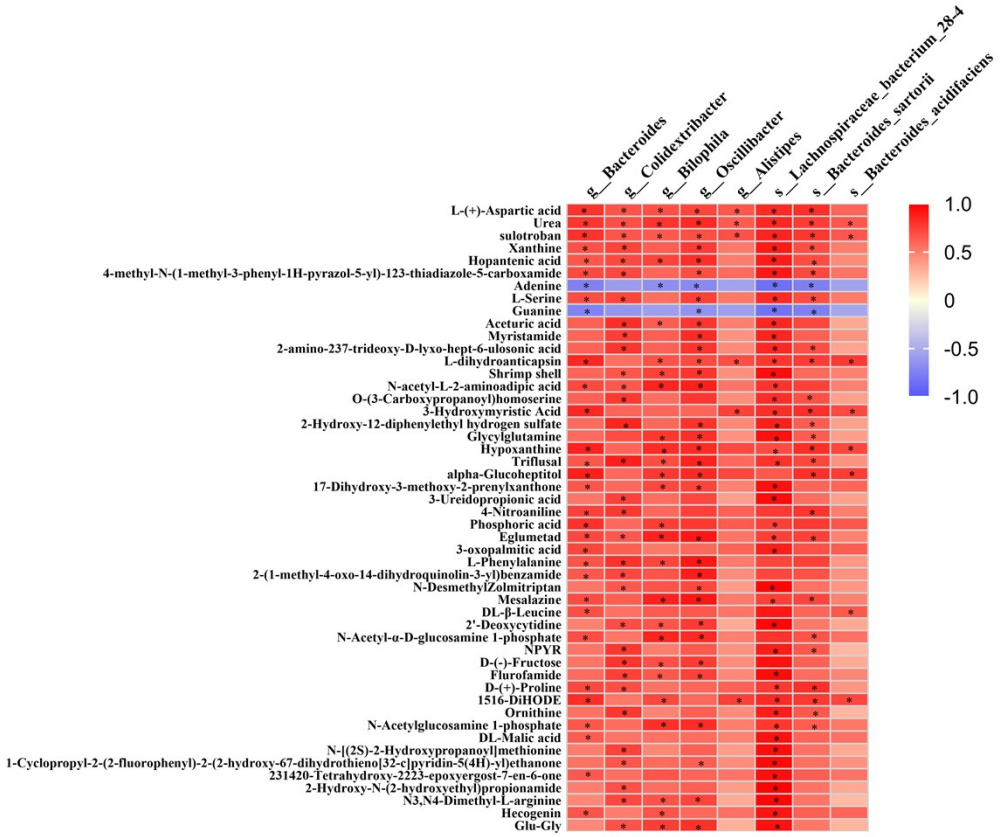

Figure 10. Correlation analysis of gut microbiota and liver metabolites in HFD and HFD+RHO mice. Red and blue indicate positive and negative correlations, respectively. *****p<0.05.